

Cite this: *RSC Adv.*, 2015, 5, 74671

## Mode of action of recombinant hypoxanthine–guanine phosphoribosyltransferase from *Mycobacterium tuberculosis*

 Paulo C. Patta,<sup>†ab</sup> Leonardo K. B. Martinelli,<sup>†a</sup> Mariane Rotta,<sup>†ac</sup> Bruno L. Abbadi,<sup>†ab</sup> Diogenes S. Santos<sup>†\*ab</sup> and Luiz A. Basso<sup>†\*ab</sup>

Tuberculosis (TB) is the second most important cause of mortality worldwide due to a single infectious agent, *Mycobacterium tuberculosis*. A better understanding of the purine salvage pathway can unveil details of the biology of *M. tuberculosis* that might be used to develop new strategies to combat this pathogen. Hypoxanthine–guanine phosphoribosyltransferase (HGPRT) is an enzyme from the purine phosphoribosyltransferase (PRTase) family and catalyzes the conversion of hypoxanthine or guanine and 5-phospho- $\alpha$ -D-ribose 1-diphosphate (PRPP) to, respectively, inosine 5'-monophosphate (IMP) or guanosine 5'-monophosphate (GMP), and pyrophosphate (PPI). Gel filtration chromatography has shown that recombinant *M. tuberculosis* HGPRT (MtHGPRT) is homodimeric. A sequential compulsory ordered enzyme mechanism with PRPP as the substrate that binds to free MtHGPRT enzyme and PPI as the first product to dissociate is proposed based on kinetic data and thermodynamics of ligand binding from isothermal titration calorimetry (ITC) results. ITC data have also provided thermodynamic signatures of non-covalent interactions for PRPP, IMP and GMP binding to free MtHGPRT. Thermodynamic activation parameters ( $E_a$ ,  $\Delta G^\ddagger$ ,  $\Delta S^\ddagger$ ,  $\Delta H^\ddagger$ ) for the MtHGPRT-catalyzed chemical reaction, pre-steady-state kinetics, solvent kinetic isotope effects, equilibrium constants and pH-rate profiles are also presented. Pre-steady-state analysis reveals that there is an initial rapid phase (burst) followed by a slower phase, suggesting that product release is rate limiting. The data here described provide a better understanding of the mode of action of MtHGPRT.

Received 27th July 2015  
Accepted 28th August 2015

DOI: 10.1039/c5ra14918e

[www.rsc.org/advances](http://www.rsc.org/advances)

## Introduction

*Mycobacterium tuberculosis* is the major etiological agent of human tuberculosis (TB) and is believed to infect one-third of the world's population. This bacteria was responsible for 8.6 million new TB cases in 2012, which resulted in 1.3 million deaths worldwide.<sup>1</sup> According to the World Health Organization (WHO), TB is the second most important cause of mortality worldwide as a single infectious agent.<sup>1</sup> Despite effective short-course chemotherapy, the increasing global burden of TB has

been associated with co-infection with human immunodeficiency virus (HIV),<sup>1,2</sup> and the emergence of multi, extensively<sup>3</sup> and recently, totally drug resistant strains of *M. tuberculosis*.<sup>4</sup>

TB is an ancient human disease,<sup>5</sup> but little is known about the nutritional adaptability of *M. tuberculosis* in the progression of TB infection.<sup>6,7</sup> It is still not clear whether *M. tuberculosis* recycles complex nutrient molecules from the human host using salvage pathways or relies on synthesis of essential molecules from passive diffusible precursors *via de novo* synthesis pathways. Purine and pyrimidine salvage pathways in *M. tuberculosis* remain an incompletely explored possibility for drug development as purine and pyrimidine biosynthesis are essential steps for the cell, supplying building blocks for DNA and RNA synthesis, among other biological roles.<sup>8</sup> Accordingly, elucidation of biochemical properties of the enzymes involved in purine and pyrimidine salvage pathways should contribute to a better understanding of the biology of *M. tuberculosis*, and, hopefully, to the design of analogs that may selectively inhibit *M. tuberculosis* replication and survival.<sup>9</sup>

The purine phosphoribosyltransferases (PRTases) form a family of enzymes that transfer 5-phosphoribosyl from 5-phospho- $\alpha$ -D-ribose 1-diphosphate (PRPP;  $\alpha$ -D-5-phosphoribosylpyrophosphate;  $\alpha$ -D-ribose diphosphate 5-phosphate) to a

<sup>a</sup>Centro de Pesquisas em Biologia Molecular e Funcional (CPBMF), Instituto Nacional de Ciência e Tecnologia em Tuberculose (INCT-TB), Pontifícia Universidade Católica do Rio Grande do Sul (PUCRS), 6681/92-A Av. Ipiranga – Tecnopuc – Prédio 92A, 90619-900, Porto Alegre, RS, Brazil. E-mail: luiz.basso@pucrs.br; diogenes@pucrs.br; Fax: +55-51-33203629; Tel: +55-51-33203629

<sup>b</sup>Programa de Pós-Graduação em Biologia Celular e Molecular, Pontifícia Universidade Católica do Rio Grande do Sul (PUCRS), 6681/12-Av. Ipiranga, 90619-900, Porto Alegre, RS, Brazil. Fax: +55-51-33203912; Tel: +55-51-33203912

<sup>c</sup>Programa de Pós-Graduação em Medicina e Ciências da Saúde, Pontifícia Universidade Católica do Rio Grande do Sul (PUCRS), 6690/30-Av. Ipiranga, 90610-000, Porto Alegre, RS, Brazil. Fax: +55-51-33203318; Tel: +55-51-33203318

<sup>†</sup> The manuscript was written through contributions of all authors. All authors have given approval to the final version of the manuscript.

nitrogen-containing nucleophile (such as the imidazole N-9 of a purine base) to form the corresponding  $\beta$ -substituted ribose 5-phosphate (such as purine nucleotides).<sup>10</sup> Despite the lack of clear sequence homology among the PRTases, these enzymes show tertiary and quaternary structure conservation.<sup>11</sup> A PPRP binding motif of 12 amino acids, which is also found in PRPP synthetases, is conserved among the PRTases involved in nucleotide synthesis or salvage pathways.<sup>12</sup> This is the main unifying characteristic of type I PRTases. The type I purine PRTase-catalyzed reactions have been found to follow a sequential ordered bi-bi mechanism, in which PRPP binds to the free enzyme followed by the purine base, and ordered PPI and nucleotide products release.<sup>13–16</sup> Another characteristic feature among the type I PRTase structures is a long flexible loop closely associated with the active site, known as “the catalytic loop”. In most of the determined structures of type I PRTase, the loop is usually highly disordered.<sup>10</sup> This PRTase family is of significant interest in both human genetic diseases and parasitic pathologies, such as Lesch–Nyhan syndrome and Chagas' disease.<sup>15–17</sup> One of the enzymes that belong to this family is the hypoxanthine–guanine phosphoribosyl-transferase (HGPRT; EC 2.4.2.8) of purine salvage pathway. HGPRTs are found in most microorganisms and mammals and their reaction involves the ribophosphorylation in one step of purine nucleobases (hypoxanthine and guanine) and their analogues to their respective nucleoside 5'-monophosphate and pyrophosphate.<sup>18</sup> HGPRT catalyzes the  $Mg^{2+}$ -dependent reversible transfer of the 5-phosphoribosyl group from PRPP to the N9 of guanine (Gua) (GPRT reaction) or hypoxanthine (Hx) (HPRT reaction) to form the corresponding ribonucleotides guanosine 5'-monophosphate (GMP) and inosine 5'-monophosphate (IMP), releasing PPI.<sup>18</sup> Investigation of purine salvage pathway enzymes of *M. tuberculosis*, including HGPRT (MthGPRT), might reveal insightful data on the complex balance that exists between the bacillus and the host.<sup>18</sup> Recently, the first crystal structure of MthGPRT has been reported.<sup>19</sup> These authors have also described acyclic nucleoside phosphonate (ANP) compounds that inhibit MthGPRT enzyme activity, and phosphoroamidates of ANPs that inhibit the growth of *M. tuberculosis*.<sup>19</sup> Incidentally, Patel and colleagues have employed computational strategies to design a series of fullerene–quinazolinones conjugates based on homology models of MthGPRT.<sup>20</sup> These compounds were synthesized and showed antibacterial activity against *M. tuberculosis*.<sup>20</sup> Accordingly, these efforts suggest that MthGPRT is a potential target for the development of chemotherapeutic agents to treat TB. However, the rational-based drug design must, preferably, rely on structural and functional data. Accordingly, efforts to elucidate the mode of action of MthGPRT appear to be warranted to improve our understanding of purine metabolism in this human pathogen, and allowing a function-based approach to also be used for MthGPRT inhibitor design efforts.

The present work describes the mode of action of recombinant MthGPRT. True steady-state kinetic parameters and isothermal titration calorimetry (ITC) data indicate that MthGPRT follows a sequential ordered mechanism. Gel

filtration data suggest a homodimeric quaternary structure for MthGPRT. Thermodynamic activation parameters ( $E_a$ ,  $\Delta G^\ddagger$ ,  $\Delta S^\ddagger$ ,  $\Delta H^\ddagger$ ) for MthGPRT-catalyzed chemical reaction, solvent kinetic isotope effects, equilibrium constant ( $K_{eq}$ ) determination, solvent kinetics isotope effects, transient kinetics measurements and pH-rate profiles results are also presented. The absolute requirement of divalent magnesium ion for catalysis, the sequential kinetic mechanism, the presence of PRPP binding motif, the homodimeric assembly in solution indicate that MthGPRT belongs to type I PRTases family of enzymes. It is hoped that the results presented here contributes to a better understanding of MthGPRT mode of action, and may also be useful to chemical biologists interested in designing loss-of-function (inhibitors) or gain-of-function (activators) chemical compounds to reveal the biological role of MthGPRT in the context of whole *M. tuberculosis* cells.

## Experimental

### Materials

All chemicals were purchased from Sigma-Aldrich (Saint Louis, USA), unless otherwise specified. The low molecular weight (LMW) and high molecular weight (HMW) Gel Filtration Calibration Kits were purchased from GE Healthcare. All kinetic data analyses were carried out using SigmaPlot 10.0 (Systac Software, Inc., Melbourne, USA). Data are presented as mean  $\pm$  standard deviation unless stated otherwise. ITC data analysis was evaluated utilizing the Origin 7 SR4 software (Microcal, Inc.). All experiments were performed at 25 °C using 50 mM 2-amino-2-hydroxymethyl-propane-1,3-diol (Tris)–HCl pH 7.4 containing 12 mM  $MgCl_2$  (buffer A), in duplicates, unless otherwise specified.

### Overexpression and purification

The recombinant MthGPRT was overexpressed and purified to homogeneity as previously described.<sup>18</sup>

### Oligomeric state determination

The oligomeric state of homogenous MthGPRT in solution was determined by size exclusion liquid chromatography on a HighLoad 10/30 Superdex-200 column (GE Healthcare). The column was pre equilibrated and the sample (100  $\mu$ L) was isocratically eluted with 1 column volume (CV) of 50 mM Tris–HCl pH 7.5 containing 200 mM NaCl at a flow rate of 0.4 mL  $min^{-1}$ . Protein elution was monitored at 215, 254, and 280 nm. The LMW and HMW Gel Filtration Calibration Kits were used as described by the manufacturer to prepare the calibration curve. The elution volumes ( $V_e$ ) of protein standards were used to calculate their corresponding partition coefficients ( $K_{AV}$ ) according to eqn (1). Blue dextran 2000 (GE Healthcare) was used to determine the void volume ( $V_0$ ) and  $V_t$  is the total bead volume of the column. The  $K_{AV}$  value for each protein was plotted *versus* the logarithm of their corresponding molecular masses, giving a linear relationship. A volume of 100  $\mu$ L (100  $\mu$ M) of MthGPRT was loaded on the gel filtration column to obtain  $V_e$ . The partition coefficient ( $K_{AV}$ ) of the recombinant

MtHPRT was calculated by data fitting to eqn (1) and its molecular mass derived from the linear relationship.

$$K_{AV} = \frac{V_e - V_o}{V_i - V_o} \quad (1)$$

### Steady-state kinetics

Recombinant MtHGPRT enzyme activity was measured by a continuous spectrophotometric assay measuring the linear increase in absorbance as a function of IMP or GMP formation in quartz cuvettes (1 cm). The experiments were performed in a UV-visible Shimadzu spectrophotometer UV2550 equipped with a temperature-controlled cuvette holder. The kinetic properties of MtHGPRT for Hx, Gua, and PRPP were spectrophotometrically determined using the difference in molar absorptivity between the nucleotide monophosphate and the free base as described for *Homo sapiens* HGPRT ( $\Delta\epsilon = 1900 \text{ M}^{-1} \text{ cm}^{-1}$  at 245 nm for IMP conversion from Hx; and  $\Delta\epsilon = 5900 \text{ M}^{-1} \text{ cm}^{-1}$  at 257.5 nm for GMP conversion from Gua).<sup>15</sup> Initial steady-state rates were calculated from the linear portion of the reaction curve under experimental conditions in which less than 5% of the substrate was consumed. True steady-state kinetics parameters were determined from initial velocity measurements for HPRT reaction varying concentrations of Hx (10–150  $\mu\text{M}$ ) at varied-fixed PRPP concentrations (200–4000  $\mu\text{M}$ ). For GPRT reaction, initial velocity measurements were determined varying concentrations of Gua (10–120  $\mu\text{M}$ ) at varied-fixed PRPP concentrations (200–3600  $\mu\text{M}$ ). All reactions started with addition of recombinant MtHGPRT, and all measurements were performed at least in duplicates. Hyperbolic saturation curves of initial rate data at single concentration of the fixed substrate and varying concentrations of the other were fitted to the Michaelis–Menten equation<sup>21</sup> (eqn (2)), in which  $v$  is the initial velocity,  $V$  is the apparent maximum initial velocity,  $A$  is the varying substrate concentration and  $K_m$  represents the apparent Michaelis–Menten constant.

$$v = \frac{VA}{K_m + A} \quad (2)$$

The  $k_{\text{cat}}$  values were calculated from eqn (3), in which  $[E]_t$  corresponds to the total concentration of enzyme subunits.

$$k_{\text{cat}} = \frac{V}{[E]_t} \quad (3)$$

Data from initial velocity measurements showing a pattern of lines intersecting to the left of the  $y$ -axis in the double-reciprocal plots (or Lineweaver–Burk plot) were fitted to eqn (4), which describes a sequential substrate binding and ternary complex formation.

$$v = \frac{VAB}{K_{ia}K_b + K_aB + K_bA + AB} \quad (4)$$

For eqn (4),  $v$  is the initial velocity,  $V$  is the true maximum initial velocity,  $A$  and  $B$  are the concentrations of the substrates,  $K_a$  and  $K_b$  are their respective Michaelis constants, and  $K_{ia}$  is the

dissociation constant for enzyme-substrate  $A$  binary complex formation.

### Isothermal titration calorimetry

ITC experiments were carried out using an iTC<sub>200</sub> Microcalorimeter (Microcal, Inc., Pittsburgh, USA). The instrument reference cell (200  $\mu\text{L}$ ) was loaded with Milli-Q water in all experiments and sample cell (200  $\mu\text{L}$ ) was filled with either 100  $\mu\text{M}$  or 80  $\mu\text{M}$  of recombinant MtHGPRT. The injection syringe (39.7  $\mu\text{L}$ ) was filled with substrates or products at different concentrations: Hx (7 mM), PRPP (10 mM), IMP (5 mM), GMP (2.5 mM) and PPI (1 mM), and the ligand isotherms were measured by direct titration (ligand into macromolecule). The same buffer preparation was used to dissolve all ligands. The stirring speed was 500 RPM at 25 °C with constant pressure for all ITC experiments. The binding reaction started with one injection of 0.5  $\mu\text{L}$  of ligand to prevent artifacts, followed by 19 injections of 2.0  $\mu\text{L}$  each at 300 s intervals. Control titrations (ligand into buffer) were performed in order to subtract the heats of dilution and mixing for each experiment prior to data analysis. The heat variation was monitored inside the cell allowing determination of binding enthalpy of the process ( $\Delta H$ ) and the equilibrium association constant ( $K_a$ ). The Gibbs free energy ( $\Delta G$ ) and the entropy ( $\Delta S$ ) of binding were calculated using the relationship described in eqn (5), in which  $R$  is the gas constant (8.324 J K<sup>-1</sup> mol<sup>-1</sup> or 1.987 cal K<sup>-1</sup> mol<sup>-1</sup>), and  $T$  is the temperature in Kelvin ( $T = \text{°C} + 273.15$ ).

$$\Delta G = -RT \ln K_a = \Delta H - T\Delta S \quad (5)$$

### Pre-steady state kinetics

Pre-steady-state kinetic measurements of the reaction catalyzed by MtHGPRT were performed to assess whether or not product release is part of the rate-limiting step. The measurements were carried out using an Applied Photophysics SX.18MV-R stopped-flow spectrofluorimeter on absorbance mode. The increase in absorbance was monitored at 245 nm for HPRT reaction and 257.5 nm for the GPRT reaction for a period of 2 seconds with 400 points (1 mm slit width = 4.65 nm spectral band) and an optical path of 2 mm. The experimental conditions were 10  $\mu\text{M}$  MtHGPRT, 12 mM MgCl<sub>2</sub>, 125  $\mu\text{M}$  Hx and 7 mM PRPP or 50  $\mu\text{M}$  Gua and 3.25 mM PRPP (mixing chamber concentrations). The control experiments were performed as the experimental conditions above in the absence of the enzyme. The dead time of the stopped-flow equipment is 1.37 ms. The pre-steady-state time course of the reaction was fitted to eqn (6) that accounts for a burst in product formation, in which  $A_{\text{obs}}$  is the (increasing) value of observed absorbance due to product formation at any time  $t$ ,  $v_0$  is the steady-state rate,  $\pi$  is the burst (rapid increase) in product formation, and  $k$  is the first-order rate constant for the rapid phase.<sup>22</sup>

$$A_{\text{obs}} = v_0t + \pi(1 - e^{-kt}) \quad (6)$$

## Energy of activation

In order to access the energy of activation ( $E_a$ ) of MthGPRT for the HPRT reaction, initial velocities were measured in the presence of saturating concentrations of Hx (150  $\mu\text{M}$ ) and PRPP (4000  $\mu\text{M}$ ). For GPRT reaction the concentrations were 120  $\mu\text{M}$  for Gua and 3600  $\mu\text{M}$  for PRPP. The measurements were carried out at temperatures ranging from 15  $^\circ\text{C}$  to 35  $^\circ\text{C}$  (from 288.15 to 308.15 K). MthGPRT was incubated for several minutes at all temperatures tested and assayed under standard conditions (buffer A) to ensure enzyme stability. The  $E_a$  was calculated from the slope ( $E_a/R$ ) of the Arrhenius plot fitting the data to eqn (7), in which  $R$  is the gas constant (8.314  $\text{J mol}^{-1} \text{K}^{-1}$ ) and the constant  $A$  represents the product of the collision frequency ( $Z$ ) and a steric factor ( $p$ ) based on the collision theory of enzyme kinetics.<sup>23</sup> Here, it is assumed a simplistic view to explain a complex phenomenon and that  $A$  is independent of temperature.

$$\ln k_{\text{cat}} = \ln A - \left(\frac{E_a}{R}\right) \frac{1}{T} \quad (7)$$

The enthalpy ( $\Delta H^\ddagger$ ), entropy ( $\Delta S^\ddagger$ ), and Gibbs free energy ( $\Delta G^\ddagger$ ) of activation were estimated using eqn (8)–(10) derived from the transition state theory of enzymatic reactions:<sup>23</sup>

$$\Delta H^\ddagger = E_a - RT \quad (8)$$

$$\Delta G^\ddagger = RT \left( \ln \frac{k_B}{h} + \ln T - \ln k_{\text{cat}} \right) \quad (9)$$

and

$$\Delta S^\ddagger = \frac{\Delta H^\ddagger - \Delta G^\ddagger}{T} \quad (10)$$

Energy values are in  $\text{kJ mol}^{-1}$ , with  $k_{\text{cat}}$  in  $\text{s}^{-1}$ , to conform to the units of the Boltzmann ( $1.3805 \times 10^{-23} \text{J K}^{-1}$ ) and Planck ( $6.6256 \times 10^{-34} \text{J s}^{-1}$ ) constants, and  $R$  is as for eqn (5). Errors on  $\Delta G^\ddagger$  were calculated using eqn (11).<sup>23</sup>

$$(\Delta G)_{\text{Err}} = \frac{RT(k_{\text{cat}})_{\text{Err}}}{k_{\text{cat}}} \quad (11)$$

## Solvent kinetic isotope effects (SKIE) and proton inventory

Solvent kinetic isotope effects were determined by measuring initial velocities for HPRT reaction using a saturating level of one substrate (Hx = 120  $\mu\text{M}$ ; PRPP = 4 mM) and varying concentrations of the other (Hx: 10–120  $\mu\text{M}$ ; PRPP: 0.32–4 mM) in either  $\text{H}_2\text{O}$  or 90%  $\text{D}_2\text{O}$ . For GPRT reaction initial velocities measurements were assayed at saturating concentration of one substrate (Gua = 50  $\mu\text{M}$ ; PRPP = 4 mM) and varying concentrations of the other (PRPP: 0.32–4 mM; Gua: 10–50  $\mu\text{M}$ ) in either  $\text{H}_2\text{O}$  or 90%  $\text{D}_2\text{O}$ . Furthermore, the reactions were performed in 50 mM Tris–HCl pH 7.4, and in 50 mM Tris–HCl pH 8.5. The proton inventory was determined using saturating concentrations of both substrates (4000  $\mu\text{M}$  PRPP and 120  $\mu\text{M}$  Hx, 3000  $\mu\text{M}$  PRPP and Gua 50  $\mu\text{M}$ ) at different mole fractions of

$\text{D}_2\text{O}$  (0–90%) in 50 mM Tris–HCl pH 7.4 and 50 mM Tris–HCl pH 8.5. Data were fitted to eqn (12), which assumes isotope effects on both  $V/K$  and  $V$ . In this equation,  $E_{V/K}$  and  $E_V$  are the isotope effects minus 1 on  $V/K$  and  $V$ , respectively, and  $F_i$  is the fraction of isotopic label in substrate  $A$ .<sup>24</sup>

$$v = \frac{VA}{K(1 + F_i E_{V/K}) + A(1 + F_i E_V)} \quad (12)$$

## Determination of equilibrium constant

To determine whether or not MthGPRT-catalyzed chemical reactions are favorable processes, the equilibrium constants ( $K_{\text{eq}}$ ) were identified at the point of equilibrium between substrates (Hx or Gua, and PRPP) and products (IMP or GMP, and PPI) for, respectively, HPRT and GPRT reactions. The  $K_{\text{eq}}$  was measured by fixing the ratio of [IMP/Hx] or [GMP/Gua] at 1 and varying the ratio of [PPI/PRPP]. For HPRT reaction, the range of [PPI/PRPP] was from 0.0033 to 0.02 (PRPP: 1000–6000  $\mu\text{M}$ ; PPI = 20  $\mu\text{M}$ ). For GPRT reaction, the range of [PPI/PRPP] was from 0.0066 to 0.025 (PRPP: 800–3000  $\mu\text{M}$ ; PPI = 20  $\mu\text{M}$ ). Specific activities ( $y$ -axis) were plotted against the ratios ( $x$ -axis) and fitted to a linear equation. The point at which the curve crosses the abscissa is equal to  $K_{\text{eq}}$  (no net enzyme-catalyzed chemical reaction). The values for the standard Gibbs free energy ( $\Delta G^\circ$ ) for MthGPRT-catalyzed chemical reactions were calculated from eqn (13), using the experimentally determined  $K_{\text{eq}}$  values, the gas constant ( $R$ ) and absolute temperature in Kelvin ( $T$ ).

$$\Delta G^\circ = -RT \ln K_{\text{eq}} \quad (13)$$

## pH-rate profiles

Prior to performing the pH-rate profiles, the recombinant enzyme stability was assessed over a wide pH range (4.5–10.5) by incubation for 2 min at 25  $^\circ\text{C}$  in 100 mM 2-( $N$ -morpholino) ethanesulphonic acid (MES)/ $N$ -2-hydroxyethylpiperazine- $N$ -2-ethanesulphonic acid (HEPES)/ $N$ -2-( $N$ -cyclohexylamino)ethanesulphonic acid (CHES) buffer mixture, and then monitoring its activity in buffer A.<sup>24</sup> The dependence of steady-state kinetic parameters on pH was determined by measuring initial velocities in the presence of varying concentrations of one substrate and saturating level of the other, in 100 mM MES/HEPES/CHES buffer, over the following pH range: for HPRT reaction, 5.5–10 (10–120  $\mu\text{M}$  varying concentrations of Hx and fixed concentration of PRPP at 4 mM, and 0.4–7 mM varying PRPP and fixed concentration of Hx at 120  $\mu\text{M}$ ); and for GPRT reaction, 5–5.5 (5–70  $\mu\text{M}$  varying concentrations of Gua and fixed concentration of PRPP at 4 mM, and 0.65–4 mM varying PRPP and fixed concentration of Gua at 70  $\mu\text{M}$ ) and 6–10 (5–35  $\mu\text{M}$  varying concentrations of Gua and fixed concentration of PRPP at 3 mM, and 0.32–3 mM varying PRPP and fixed concentration of Gua at 35  $\mu\text{M}$ ). All measurements were performed at least in duplicates.

The pH-rate profile was generated by plotting logarithm value of  $k_{\text{cat}}$  or  $k_{\text{cat}}/K_m$  of the substrates *versus* the pH values (5.5 to 10) and data were fitted to eqn (14), in which  $y$  is the apparent kinetic parameter ( $\log k_{\text{cat}}$  or  $\log k_{\text{cat}}/K_m$ ),  $C$  is the pH-



independent plateau value of  $y$ ,  $H$  is the hydrogen ion concentration, and  $K_a$  is the apparent acid dissociation constant for the ionizing group.

$$\log y = \log \left( \frac{C}{1 + \frac{H}{K_a}} \right) \quad (14)$$

## Result and discussion

### Oligomeric state determination

In order to determine the oligomeric state of the enzyme, MthGPRT (100  $\mu\text{M}$ ) was loaded on a Superdex 200 HR 10/30 size exclusion column. The protein elution profile and data fitting to eqn (1) yielded an apparent molecular mass value of 46 kDa. As the MthGPRT subunit molecular mass value is 22.251 kDa, the gel filtration result suggests that MthGPRT is a homodimer in solution, which suggests that this enzyme belongs to type I PRTases as enzymes of this family are homodimers.<sup>25</sup> It has recently been reported that MthGPRT enzyme in complex with GMP, Ppi and  $\text{Mg}^{2+}$  crystallized as a tetramer.<sup>19</sup> This result is in disagreement with both the dimeric state of MthGPRT in solution described here and other type I PRTases, which are homodimers in solution.<sup>25</sup> Interestingly, the crystal structure of MthGPRT in complex with an aza-acyclic bisphosphonate containing a guanine base crystallized as a dimer.<sup>19</sup> A mechanism has been put forward in which interactions between Tyr93 in the mobile loop (residues 90–106) of one subunit and Arg141

and C-terminal amino acids of the mobile loop of an adjacent subunit of MthGPRT have to be broken for catalysis.<sup>19</sup> Disruption of these interactions would result in the mobile loop closing over the MthGPRT active site for catalysis as proposed for other 6-oxopurine PRTases.<sup>19</sup> Interestingly, this proposal would imply that there would be two forms of MthGPRT in solution: an inactive tetrameric form and an active dimeric one. Whether or not there is an equilibrium between two forms of MthGPRT in solution will have to await for further evidence. Notwithstanding, the results here reported show that recombinant MthGPRT is an active dimer in solution.

### Steady-state kinetics

The initial velocity experiments allowed the calculation of the true steady-state kinetics parameters and a proposal of the enzyme mechanism. The double-reciprocal plots showed a pattern of lines intersecting to the left of the  $y$ -axis (Fig. 1), which is consistent with a sequential mechanism for the forward reaction. The data were thus fitted to eqn (4), yielding the true macroscopic steady-state kinetic constants for the forward reaction of MthGPRT (Table 1). Divalent metal ion activation of substrate PRPP has already been demonstrated as essential for PRTase catalyzed reactions<sup>26–28</sup> in which the dimagnesium  $\text{Mg}_2\text{PRPP}$  complex (and not PRPP alone) was proved to be the true substrate for HGPRT reaction.<sup>28</sup> No activity could be detected when  $\text{Mg}^{2+}$  was omitted from the reaction mixture for the MthGPRT (data not shown). These results are in agreement with MthGPRT belonging to type I PRTases, for

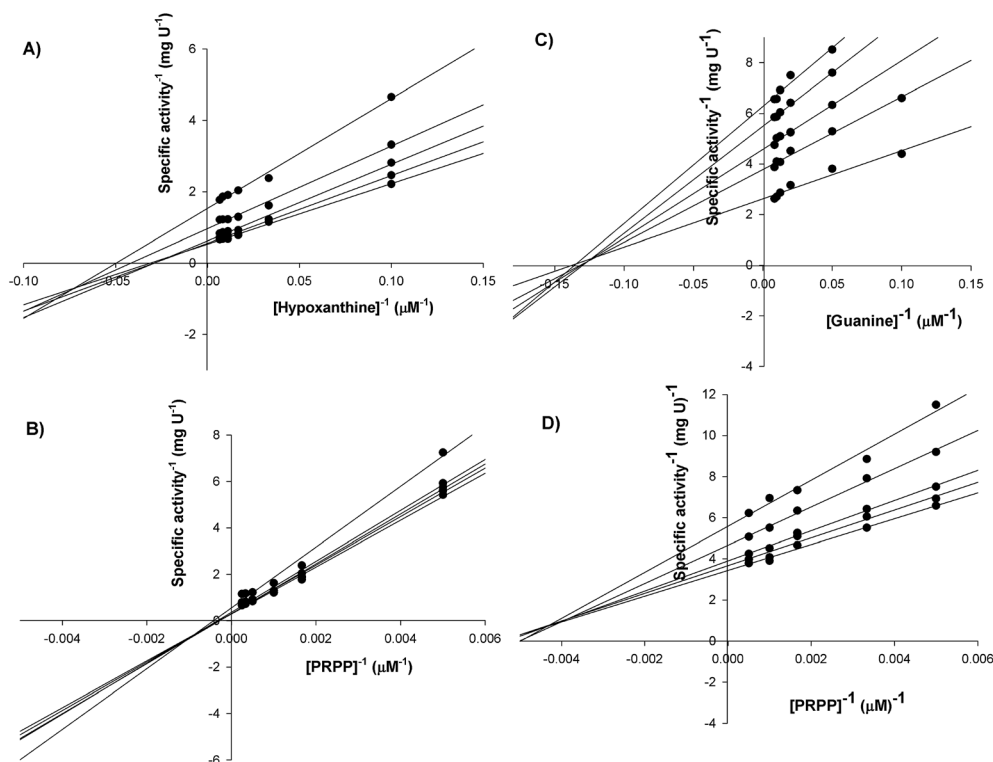


Fig. 1 Intersecting initial velocity patterns for MthGPRT using either Hx or PRPP (A and B), and Gua or PRPP (C and D) as the variable substrate. Each curve represents varied-fixed levels of the co-substrate.

Table 1 True steady-state kinetic parameters for MthGPR1

Substrate	$K_m$ ( $\mu\text{M}$ )	$V_{\text{max}}$ ( $\text{U mg}^{-1}$ )	$k_{\text{cat}}$ ( $\text{s}^{-1}$ )	$k_{\text{cat}}/K_m$ ( $\text{M}^{-1} \text{s}^{-1}$ )
Hypoxanthine	$26 \pm 2$	$2.40 \pm 0.09$	$0.89 \pm 0.04$	$3.4 (\pm 0.3) \times 10^4$
PRPP <sup>a</sup>	$14.1 (\pm 0.4) \times 10^2$	—	—	$6.3 (\pm 0.5) \times 10^2$
Guanine	$10 \pm 1$	$0.52 \pm 0.01$	$0.193 \pm 0.004$	$1.9 (\pm 0.2) \times 10^4$
PRPP <sup>b</sup>	$6.5 (\pm 0.7) \times 10^2$	—	—	$2.9 (\pm 0.3) \times 10^2$

<sup>a</sup> HPRT reaction. <sup>b</sup> GPRT reaction.

which there is an absolute requirement of divalent magnesium ion for catalysis.<sup>25</sup>

The steady-state kinetics constants for MthGPR1 (Table 1) showed an approximately 54-fold larger value for  $K_m$  of PRPP as compared to Hx, and 65-fold as compared to Gua. Higher overall  $K_m$  values for PRPP compared to Hx or Gua have also been reported for *Homo sapiens* (HsHGPR1) (68-fold for Hx; 18-fold for Gua)<sup>15</sup> and *Plasmodium falciparum* (PfHGPR1) (27-fold for Hx; 53-fold for Gua).<sup>29</sup> MthGPR1 showed a  $K_m$  2.6-fold lower for Gua as compared to Hx. However, the  $k_{\text{cat}}/K_m$  value was 1.8-fold larger for the HPRT reaction as compared to the GPRT reaction. As  $k_{\text{cat}}/K_m$  determines the specificity for competing substrates, MthGPR1 appears to be more efficient at using Hx than Gua as co-substrate. Interestingly, HsHGPR1 has a  $k_{\text{cat}}/K_m$  value of  $1.3 \times 10^7 \text{ M}^{-1} \text{ s}^{-1}$  for HPRT reaction and  $3.7 \times 10^6 \text{ M}^{-1} \text{ s}^{-1}$  for GPRT reaction,<sup>15</sup> indicating a higher efficiency at using both substrates when compared to MthGPR1. As for MthGPR1, the apparent second-order rate constant value for HsHGPR1-catalyzed phosphoribosyl transfer to Hx is larger than to Gua.

The double reciprocal patterns of lines intersecting to the left of the y-axis (Fig. 1) suggest that the reaction catalyzed by MthGPR1 obeys a sequential (either random or ordered) kinetic mechanism, which leads to the formation of a ternary complex capable of undergoing catalysis.<sup>24</sup> Sequential mechanisms have been suggested as one of the features shared by type I PRTases.<sup>25,27,30–32</sup> The pattern of lines intersecting to the left of the y-axis rules out ping-pong (parallel lines), steady-state random (that gives non-linear reciprocal plots), and rapid-equilibrium ordered (one of the family of lines should cross at a single value on the y-axis) mechanisms. However, the double-reciprocal plots alone cannot distinguish between rapid-equilibrium random and steady-state compulsory ordered bi bi mechanisms. Accordingly, ITC studies were performed to distinguish between these enzyme mechanisms.

### Isothermal titration calorimetry

As double reciprocal plots suggested a sequential kinetic mechanism, substrate(s) and product(s) binding processes were assayed by ITC at 25 °C to ascertain the order, if any, of chemical compound addition. The measure of heat taken up or released upon binding of a ligand provides the binding enthalpy ( $\Delta H$ ) of the process, an estimate for the stoichiometry of the interaction ( $n$ ) and the equilibrium binding constant ( $K_a$ ). These values allow the Gibbs free energy ( $\Delta G$ ) and the entropy ( $\Delta S$ ) of the process to be calculated, as well as the dissociation constant at

equilibrium ( $K_d$ ) from reciprocal of  $K_a$ . The ITC data for binding of ligands to MthGPR1 are summarized in Table 2. These binding assays showed that PRPP, IMP and GMP can bind to free MthGPR1 (Fig. 2A–C). ITC data for these compounds were fitted to one set of sites model. No significant heat change upon titration of Hx and PPI to MthGPR1 was detected under the experimental conditions for ITC measurements (data not shown).

Formation of MthGPR1:IMP and MthGPR1:GMP binary complexes (Fig. 2B and C) were detected by ITC measurements and generated exothermic profiles (heat released to the system). On the other hand, formation of MthGPR1:PRPP binary complex (Fig. 2A) was characterized by an endothermic profile (heat taken up from the system). No binding of either Hx or PPI to free MthGPR1 was detected (data not shown). Fitting the ITC data for PRPP, IMP and GMP binding to free MthGPR1 to one set of sites binding model yielded  $n$  values (number of active sites) of 1.81 sites per monomer for GMP, 12 for PRPP and fixed as 1 for IMP. This value indicates the number of molecules bound to each enzyme active site with equal affinity. The value of 12 to stoichiometry ( $n$ ) of the PRPP binding to the free MthGPR1 might be related to the instability and purity of the compound (75% according to the supplier). It should be pointed out that binding of Gua could not be evaluated by ITC studies due to limited solubility in aqueous solutions. Incidentally, attempts were made to measure whether or not Gua binds to free MthGPR1 enzyme using protein fluorescence spectroscopy; however, no reliable data could be obtained due to high inner filter effects (data not shown). Accordingly, here it is assumed that the lack of binding of Hx to free enzyme serves as a surrogate to Gua (no binding to free MthGPR1), and thus the same kinetic mechanism is likely followed by both HPRT and GPRT reactions. The ITC measurements provided dissociation constants values ( $K_d$ ) for IMP (130  $\mu\text{M}$ ) and GMP (2.1  $\mu\text{M}$ )

Table 2 Binding parameters for MthGPR1 from ITC titration assays

	PRPP	GMP	IMP
$\Delta G$ ( $\text{kcal mol}^{-1}$ )	$-5.9 (\pm 0.1)$	$-7.7 (\pm 0.1)$	$-5.3 (\pm 0.2)$
$\Delta S$ ( $\text{cal mol}^{-1} \text{K}^{-1}$ )	$20.5 (\pm 0.4)$	$-3.94 (\pm 0.03)$	$-38 (\pm 2)$
$\Delta H$ ( $\text{kcal mol}^{-1}$ )	$0.205 (\pm 0.004)$	$-8.9 (\pm 0.1)$	$-16.7 (\pm 0.9)$
$K_a$ ( $\text{M}^{-1}$ )	$2.2 (\pm 0.3) \times 10^4$	$4.8 (\pm 0.5) \times 10^5$	$7 (\pm 1) \times 10^3$
$K_d$ ( $\mu\text{M}$ )	$48 (\pm 7)$	$2.1 (\pm 0.2)$	$1.3 (\pm 0.2) \times 10^2$

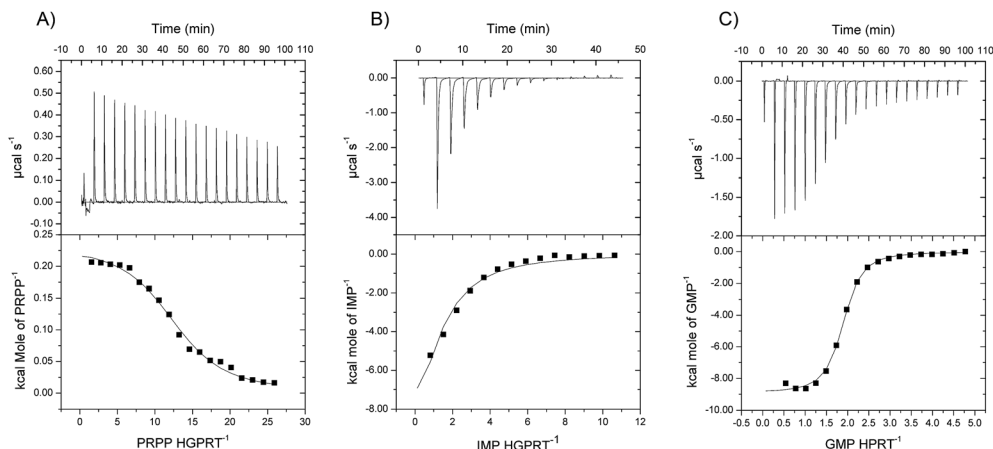


Fig. 2 Ligand binding assays for binary complex formation: PRPP (A), IMP (B) and GMP (C). ITC data were fitted to one set of sites binding model.

(Table 2). A larger value for IMP as compared to GMP has also been observed for HsHGPRT.<sup>15</sup>

These ITC results and double-reciprocal plots suggest a sequential compulsory ordered mechanism for MthGPR1, in which PRPP binds to free enzyme followed by Hx or Gua binding; and PPI is the first product to dissociate followed by the respective monophosphate nucleoside (IMP or GMP) release, leading to the regeneration of free enzyme (Fig. 3). A sequential mechanism has been proposed for HsHGPRT,<sup>15</sup> in which PRPP binds first and release of the nucleotide as the last step of the reaction. Sequential mechanisms have also been suggested for others type I PRTases.<sup>27,33</sup>

The ITC results showed significant heat changes upon ligand (PRPP, IMP, or GMP) binding to free MthGPR1 enzyme (Fig. 2), thereby providing thermodynamic signatures of non-covalent interactions to each binding process. Observed enthalpies arise largely as a result of changes in interatomic interactions (*e.g.*, hydrogen bonds and/or van der Waals interactions), in which the sign indicates whether there is a net favourable (negative  $\Delta H$ ) or unfavourable (positive  $\Delta H$ ) redistribution of the network of interactions between the reacting species (including solvent).<sup>34</sup> Hydrophobic interactions are related to the relative degrees of disorder in the free and bound systems and thus these interactions are reflected in the entropy change. The release of “bound” water molecules from a surface to the bulk solvent is usually a source of favourable entropy (positive  $\Delta S$ ). A reduction in conformational states in either ligand or protein upon binary complex formation is entropically unfavourable (negative  $\Delta S$ ) because this molecular recognition process limits the external rotational and translational freedom of both partners (for instance, structuring regions of the protein

adjacent to the bound ligand and loss of conformational freedom of free ligand).<sup>34</sup> The negative  $\Delta H$  values for IMP and GMP binding (Table 2) indicate that these processes are accompanied by favourable redistribution of H-bonds and/or van der Waals interactions. The negative  $\Delta S$  values for these binding processes are likely coupled to a decrease in conformational states upon binary complex formation. Accordingly, IMP or GMP dissociation from the binary complex to yield free MthGPR1 enzyme is likely to be accompanied by an increase in conformational states including the flexible loop involved in binding of nitrogenous base, which is a characteristic feature of type I PRTases.<sup>25</sup> The ITC data also show that GMP binds 68-fold more strongly than IMP, probably due to additional interactions made by the exocyclic amino group of GMP and MthGPR1.<sup>15</sup> The thermodynamic analysis of binding of PRPP gives a  $K_d$  of 48  $\mu\text{M}$ , with favourable entropic contribution and unfavourable binding enthalpy (Table 2), indicating that this binding event is likely accompanied by release of water molecules to bulk solvent and unfavourable redistribution of the hydrogen bond network and/or van der Waals interactions between the reacting species.<sup>34</sup>

The Gibbs free energy values for PRPP, GMP and IMP binding to MthGPR1 (Table 2) show that these processes are favourable (negative value for  $\Delta G$ ). As indicated in eqn (5),  $\Delta G$  consists of enthalpic and entropic contributions, and the results given in Table 2 are yet additional examples of entropy–enthalpy compensation often observed in biomolecular interactions.<sup>35</sup> If the ligand displays a significant enthalpic contribution, sometimes this contribution is offset by a large entropic compensation, which happens when we compare the Gibbs free energy of binding of substrate and products to MthGPR1. For GMP and IMP binding, favorable formation of hydrogen bond and/or van der Waals interactions are accompanied by a likely decrease in conformational states of enzyme and ligand species, thus compensating all gain in the enthalpy. On the other hand, for PRPP the inverse happens: the unfavourable redistribution of the hydrogen bonds is compensated by favorable entropic contribution (*e.g.*, release of “bound” water molecules to solvent), compensating the penalty in enthalpy.<sup>35</sup>

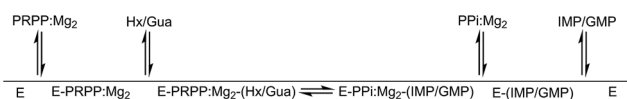


Fig. 3 Proposed kinetic enzyme mechanism for MthGPR1. This order of substrate binding and product release is suggested on basis of the Lineweaver–Burk plots (kinetics) and thermodynamics.

## Energy of activation

The energy of activation for the enzyme-catalyzed chemical reaction was assessed by measuring the dependence of  $k_{\text{cat}}$  on temperature for Hx and Gua (Fig. 4). These data were fitted to eqn (7). The results presented in Table 3 are derived from data fitting to eqn (7)–(11). These results provide the energy of activation ( $E_a$ ), as well as the transition state enthalpy ( $\Delta H^\ddagger$ ), entropy ( $\Delta S^\ddagger$ ) and Gibbs free energy ( $\Delta G^\ddagger$ ).

The linearity of the Arrhenius plot (Fig. 4) suggests that there is no change in the rate-limiting step over the temperature range utilized in the assay for HPRT and GPRT reactions.<sup>21</sup> The  $E_a$  values for Hx and Gua, representing the minimum amount of energy necessary to initiate the MthGPRT-catalyzed chemical reaction, were similar (Table 3). The values of free activation energy ( $\Delta G^\ddagger$ ) represent the energy barrier required for reactions to occur. The  $\Delta G^\ddagger$  values can also be regarded as the variation of the Gibbs energy between the enzyme:substrate(s) activated complex and enzyme:substrate(s) complex in the ground state. No differences in  $\Delta G^\ddagger$  values were observed for the substrates studied here, suggesting a similar overall free activation energy for HPRT and GPRT reactions. The constant  $A$  of eqn (7) corresponds to the product of collision frequency ( $Z$ ) and the probability or steric factor ( $p$ ) from the collision theory of reaction rates. From the absolute rate theory,  $A = pZ = (k_B T/h) e^{\Delta S^\ddagger/R}$ . Accordingly, this equation enables interpretation of the probability factor in terms of entropy of activation. The negative values for the entropy of activation ( $\Delta S^\ddagger$ ) for HPRT and GPRT reactions (Table 3) suggests that these reactions proceed slower

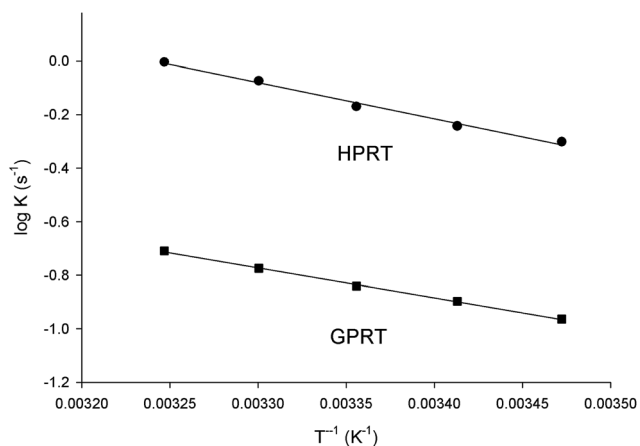


Fig. 4 Arrhenius plot for Hx and Gua substrates (temperature dependence of  $\log k_{\text{cat}}$ ).

Table 3 Thermodynamic activation parameters for MthGPRT<sup>a</sup>

Parameter	HPRT	GPRT
$E_a$ ( $\text{kcal mol}^{-1}$ )	$6.20 \pm 0.09$	$5.10 \pm 0.03$
$\Delta H^\ddagger$ ( $\text{kcal mol}^{-1}$ )	$5.60 \pm 0.08$	$4.50 \pm 0.02$
$\Delta S^\ddagger$ ( $\text{cal mol}^{-1} \text{K}^{-1}$ )	$-39.6 \pm 0.5$	$-46.6 \pm 0.2$
$\Delta G^\ddagger$ ( $\text{kcal mol}^{-1}$ )	$17 \pm 0.2$	$18 \pm 0.1$

<sup>a</sup> All values were determined at 25 °C (298.15 K).

than predicted by the collision theory and that the entropy value for the enzyme:substrate(s) activated complex is lower than the one for enzyme:substrate(s) in the ground state (there is loss of degrees of freedom on going from the ground state to activated state).

## Pre-steady state kinetics

To determine whether product release contributes to the rate limiting step, pre-steady-state analysis of the reaction catalyzed by MthGPRT was performed. Fitting the pre-steady-state data to eqn (6), which describes an initial rapid phase followed by a slower linear phase, yielded a value of  $1249 (\pm 40) \text{ s}^{-1}$  for the first-order rate constant and a value of  $0.0027 (\pm 1 \times 10^{-5}) \text{ s}^{-1}$  for the steady-state rate of HPRT reaction (Fig. 5A), and a value of  $1024 (\pm 32) \text{ s}^{-1}$  for the first-order rate constant and a value of  $0.0030 (\pm 7 \times 10^{-5}) \text{ s}^{-1}$  for the steady-state rate of GPRT reaction (Fig. 5B). The first-order constant values for the rapid phase for both reactions are larger than the steady-state rate, suggesting fast formation of products in the MthGPRT active site followed by a slow rate-limiting step. The rates for the initial rapid phase are likely faster than measured by the stopped-flow experiment as the absorbance of control experiments indicate that part of the signal was not detected. Hence, the burst observed in the initial phase represents a fraction of the stopped-flow signal as the remaining was lost in the dead-time of the equipment. The observable fraction of the curve depends on the relationship between the reaction rate and the dead-time, in which the observed change ( $x_{\text{obs}}$ ), total change ( $x_{\text{tot}}$ ), the dead-time ( $t_d$ ) and the rate constant ( $k$ ) can be described by the following equation:  $kt_d = \ln(x_{\text{tot}}/x_{\text{obs}})$ .<sup>22</sup> This analysis indicates that the rate for the initial rapid phase is at least  $1930 \text{ s}^{-1}$  for HPRT and  $1890 \text{ s}^{-1}$  for GPRT reactions. These results are in good agreement with stopped-flow data fitting to eqn (6) ( $1249 \text{ s}^{-1}$  and  $1024 \text{ s}^{-1}$  for HPRT and GPRT reactions respectively).

The value of  $0.0027 \text{ s}^{-1}$  for change in absorbance at 245 nm for the linear phase in the pre-steady-state experiment for the HPRT reaction corresponds to approximately  $0.71 \text{ s}^{-1}$  (using  $\Delta\epsilon = 1900 \text{ M}^{-1} \text{ cm}^{-1}$ , optical path of 2 mm, and MthGPRT concentration of  $10 \mu\text{M}$ ). The value of  $0.0030 \text{ s}^{-1}$  for the GPRT reaction corresponds to approximately  $0.25 \text{ s}^{-1}$  ( $\Delta\epsilon = 5900 \text{ M}^{-1} \text{ cm}^{-1}$  at 257.5 nm, optical path of 2 mm, and MthGPRT concentration of  $10 \mu\text{M}$ ). These values are in reasonable good agreement with the  $k_{\text{cat}}$  values determined by initial velocity measurements in steady-state kinetics ( $0.89 \text{ s}^{-1}$  and  $0.19 \text{ s}^{-1}$  for, respectively, HPRT and GPRT reactions).

The observation of burst in product formation in the time course of the transient phase suggests rapid formation and build-up of products in the MthGPRT active sites.<sup>22</sup> If a burst is observed during the transient phase, and the concentration of IMP or GMP produced is approximately equal to free initial MthGPRT subunit concentration, it would indicate that the chemical step of the reaction is much faster than the release of product(s) (PPi, IMP or GMP). The size of the burst phases for HPRT and GPRT reactions are  $40 \mu\text{M}$  and  $10 \mu\text{M}$  of product formed before being released from the active sites of MthGPRT to solution (Fig. 5). As the concentration of enzyme used in the



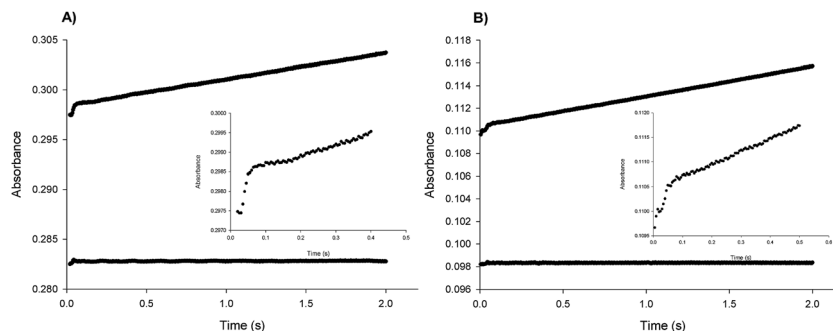


Fig. 5 Stopped-flow trace for product formation by measuring the increase in absorbance at 245 nm for HPRT (A) and 257.5 nm for GPRT (B) reactions. Data were fitted to eqn (6) for an initial rapid phase followed by a linear phase. The inset represents the biphasic profile of the experiment in a smaller scale of time (500 ms).

experiment was 10  $\mu\text{M}$ , it can be concluded that release of product(s) and/or any step linked to it (*e.g.*, enzyme conformational changes) contribute to the rate-limiting step in the mode of action of MtHGPRT. A burst in IMP and GMP product formation has also been observed for human HGPRT in rapid quench experiments,<sup>15</sup> which prompted the authors to propose that phosphoribosyl transfer is fast and that release of the nucleotide product (IMP or GMP) limits the overall rate for the forward reaction.<sup>15</sup>

### Solvent kinetics isotope effects (SKIE) and proton inventory

To evaluate the contribution of proton transfer from the solvent to the rate of phosphoribosyl transfer of MtHGPRT-catalyzed reaction, SKIE were determined by data fitting to eqn (12), yielding the results given in Table 4. Isotope effects on  $V$  report on events following the ternary complex formation capable of undergoing catalysis (fully loaded enzyme), which include the chemical steps, possible enzyme conformational changes, and product release (leading to regeneration of free enzyme). Solvent isotope effects on  $V/K$  report on the contribution of the proton transfer in steps in the reaction mechanism from binding of the isotopically labeled chemical compound (solvent) to the first irreversible step, usually considered to be the release of the first product (that is, all rate constants from reactant binding until the first irreversible step).<sup>36</sup> Accordingly, to evaluate the contribution, if any, of proton transfer from solvent to a rate-limiting step, measurements of solvent isotope effects on  $V$  and  $V/K$  were carried out. As rule of thumb, deuterium accumulates where binding is tighter (that is, fractionation factor is larger than one). Transition state proton contributes the reciprocal of its respective fractionation factor to the solvent isotope effect, whereas the contribution of a reactant state proton to the solvent isotope effect is equal to its fractionation factor.<sup>37</sup> Although isotope effects measurements are to be carried out at pH values in which  $V$  and  $V/K$  values are not dependent on pH, we deemed appropriate to determine SKIE and proton inventory at pH values of 7.4 and 8.5. The former would more closely mimic the pH value found in the context of whole cell, and the latter to provide data for solvent isotope effects at a pH value in which the steady-state kinetic

parameters are independent of pH (as will be shown below in the pH-rate profiles).

For the experiments performed at pH 7.4 (Table 4), the SKIE parameters for HPRT reaction ( $^{D_2}O V_{PRPP}$ ,  $^{D_2}O V/K_{PRPP}$ ,  $^{D_2}O V_{HX}$ ,  $^{D_2}O V/K_{HX}$ ) suggest modest, if any, participation of the proton solvent in catalysis and binding. At pH 8.5 (Table 4), the SKIE results show the similar effects for  $^{D_2}O V_{PRPP}$ ,  $^{D_2}O V/K_{PRPP}$ , and  $^{D_2}O V_{HX}$ , whereas  $^{D_2}O V/K_{HX}$  is inverse. The SKIE for GPRT reaction ( $^{D_2}O V/K_{PRPP}$ ,  $^{D_2}O V_{Gua}$ ,  $^{D_2}O V/K_{Gua}$ ) also suggest modest, if any, participation of proton transfer from the solvent in catalysis and binding at pH 7.4 (Table 4). At pH 8.5, the SKIE for GPRT reaction show similar effects (as compared to pH 7.4) for  $^{D_2}O V/K_{PRPP}$ ,  $^{D_2}O V_{Gua}$ , and  $^{D_2}O V/K_{Gua}$  (Table 4). However, there is an inverse effect for  $^{D_2}O V_{PRPP}$  at pH 7.4 ( $0.71 \pm 0.04$ ) that is negligible at pH 8.5 ( $1.04 \pm 0.04$ ) for the GPRT reaction. Before trying to interpret these results, it should be pointed out that there have been reported inverse isotope effects on  $V$  or  $V/K$  of unknown origin.<sup>38,39</sup> The expression of deuterium kinetic isotope effect on  $V$  includes the intrinsic isotope effect, commitment factors (forward and reverse) and equilibrium isotope effect.<sup>37</sup> The inverse effect on  $^{D_2}O V_{PRPP}$  at pH 7.4 suggests that deuterium accumulates (tighter binding) in a transition state from ternary complex to the first irreversible step as transition state protons contribute the reciprocal of its fractionation factor to the kinetic solvent isotope effect (providing equilibrium isotope effect is normal). Yet at pH 8.5, the inverse SKIE  $^{D_2}O V_{PRPP}$  at pH 7.4 has become a modest, if any, normal contribution of the proton solvent in catalysis and binding. It has been pointed out that the rate limitation of the chemical

Table 4 Solvent kinetic isotope effect for MtHGPRT

Parameter	SKIE pH 7.4	SKIE pH 8.5	Comments
$^{D_2}O V_{PRPP}$	$1.2 \pm 0.1$	$1.24 \pm 0.07$	HPRT
$^{D_2}O V/K_{PRPP}$	$1.3 \pm 0.2$	$0.95 \pm 0.13$	HPRT
$^{D_2}O V_{HX}$	$1.09 \pm 0.08$	$1.3 \pm 0.1$	HPRT
$^{D_2}O V/K_{HX}$	$1.3 \pm 0.3$	$0.7 \pm 0.2$	HPRT
$^{D_2}O V_{PRPP}$	$0.71 \pm 0.04$	$1.04 \pm 0.04$	GPRT
$^{D_2}O V/K_{PRPP}$	$0.9 \pm 0.2$	$0.74 \pm 0.09$	GPRT
$^{D_2}O V_{Gua}$	$0.92 \pm 0.07$	$0.98 \pm 0.04$	GPRT
$^{D_2}O V/K_{Gua}$	$0.8 \pm 0.3$	$0.78 \pm 0.01$	GPRT

step can vary as the pH changes, and the degree of the isotope effects on  $V$  and  $V/K$  may change depending on the contribution of the isotope-sensitive step to overall rate limitation at saturating and limiting reactant concentrations, respectively.<sup>24</sup>

Proton inventory studies were performed at pH 7.4 and pH 8.5 at saturating concentrations of substrates (Fig. 6). To rule out any effect that elevate mole fraction of D<sub>2</sub>O might have on the ionization constants of assay buffer, the pH of the reaction mixtures containing the highest concentration of D<sub>2</sub>O (90%) was measured. No pH change in the presence of D<sub>2</sub>O was observed, indicating that the use of equivalent buffers (concentrations of all solutes are the same) guaranteed that rates were being measured at equivalent positions on the pH and pD-rate profiles.<sup>37</sup> The proton inventory data show that the modest SKIE on  $V$  (Table 4) arises from a single protonic site (Fig. 6). In agreement with the SKIE on  $V$  (Table 4), a modest normal effect with a single protonic site involvement was observed for the HPRT reaction at pH 7.4 (Fig. 6A) and at pH 8.5 (Fig. 6A-inset). For the GPRT reaction, no protonic site involvement was observed at pH 8.5 (Fig. 6B-inset), whereas at pH 7.4 a modest normal effect suggests limited participation, if any, of a single protonic site on  $V$  (Fig. 6B). Solvent isotope effects lead to isotope exchanges at hundreds of protic positions of the enzyme, which precludes any assignment to a particular chemical group.

### Determination of equilibrium constant

Plotting the MthGPRT enzyme activity as a function of [PPI]/[PRPP] ratio gives a straight line for HPRT and GPRT reactions (Fig. 7). The analysis of the equilibrium experiments for HPRT and GPRT reactions yielded values of 0.0271 for  $K_{\text{eq}}$  of Hx (Fig. 7A) and 0.0357 for  $K_{\text{eq}}$  of Gua (Fig. 5B). The standard free energy ( $\Delta G^\circ$ ) can thus be calculated by eqn (13). This analysis gives values for  $\Delta G^\circ$  at 25 °C (298.15 K) of 8.95 kJ mol<sup>-1</sup> (2.13 kcal mol<sup>-1</sup>) for Hx and 8.27 kJ mol<sup>-1</sup> (1.97 kcal mol<sup>-1</sup>) for Gua. These results suggest that HPRT and GPRT reactions are not favorable processes at equilibrium. The PRTase reactions display a wide range of  $K_{\text{eq}}$ , from 0.1 for OPRTase to a value of 300 for APRTase.<sup>15</sup> However, to show whether or not phosphoribosyl transfer is a favorable process ( $\Delta G < 0$ ) *in vivo*, the

intracellular concentrations of substrates and products need to be determined. There are other *M. tuberculosis* enzymes that catalyze reactions that could provide free bases and PRPP. For instance, purine nucleoside phosphorylase (PNP), involved in the metabolism of both purine and pyrimidine.<sup>40</sup> PNP catalyzes the reversible phosphorolysis of the *N*-glycosidic bond of  $\alpha$ -purine (deoxy)ribonucleosides to generate  $\beta$ -(deoxy)ribose 1-phosphate and the corresponding purine bases.<sup>41,42</sup>

### pH-rate profile

To probe for acid–base catalysis and likely residues involved in catalysis and/or substrate binding, pH-rate profiles were determined for the steady-state kinetic parameters of MthGPRT. In this experiment, initial velocities measurements were assayed in a broad range of pH values. The pH-rate profiles are shown in Fig. 8. Data from the pH-rate profile of HPRT reaction for  $k_{\text{cat}}$  and  $k_{\text{cat}}/K_{\text{PRPP}}$  were fitted to eqn (14), yielding values of, respectively, 6.3 ( $\pm 1.2$ ) and 7.0 ( $\pm 0.9$ ) (Fig. 8A). For the GPRT reaction, data fitting to eqn (14) yielded a value of 6.1 ( $\pm 2.8$ ) for  $k_{\text{cat}}/K_{\text{PRPP}}$  and 6.8 ( $\pm 2.0$ ) for  $k_{\text{cat}}/K_{\text{Gua}}$  (Fig. 8B). There appears to be no obvious ionizing group to be predicted from the  $k_{\text{cat}}/K_{\text{Hx}}$  data for HPRT reaction, and, interestingly,  $k_{\text{cat}}$  data for GPRT reaction (Fig. 8A and B). The enzyme was stable over the pH range (HPRT reaction: 5.5–10; GPRT reaction: 5–10) used in pH-rate profiles (data not shown).

The pH dependence of  $k_{\text{cat}}$  is concerned with the chemical step and its value follows the  $\text{p}K_{\text{a}}$  of groups that play critical roles in catalysis. The pH-rate data of  $k_{\text{cat}}$  for HPRT reaction showed a profile of a curve with slope of +1 that goes to zero as a function of increasing pH values (Fig. 8A). In HsHGPRT, Asp137 (Asp126 in MthGPRT) has been proposed to act as a general acid/base for catalysis.<sup>43</sup> Although attempts of fitting the pH-rate data of  $k_{\text{cat}}$  for GPRT reaction (Fig. 8B) to an equation that describes “hollows” were made,<sup>44</sup> no convergence to any parameters could be achieved. A similar profile was shown for the HPRT reaction catalyzed by HsHGPRT enzyme.<sup>43</sup> Xu and Grubmeyer concluded that this “hollow” possibly arises from slow protonic equilibria for this reaction, in which there are slow proton transfers between enzymatic residues and solvent.<sup>43</sup> The possible role of Asp126 in the chemical mechanism of

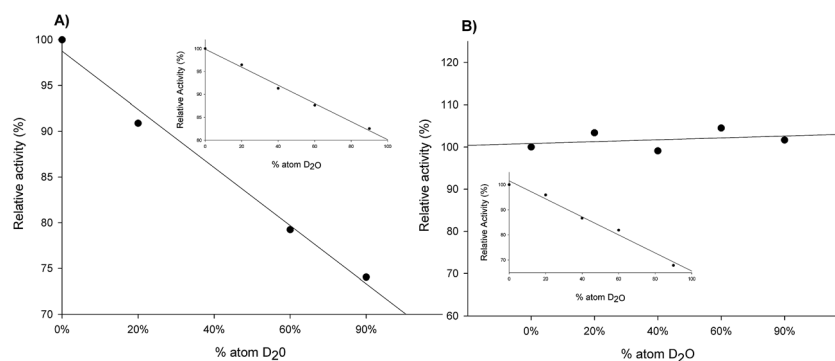


Fig. 6 Proton inventory at different mole fractions of D<sub>2</sub>O (0–90%). Enzyme activity measurements were carried out at saturating concentrations of substrates. (A) HPRT reaction: 4000  $\mu\text{M}$  PRPP and 120  $\mu\text{M}$  Hx at pH 7.4. (B) GPRT reaction: 3000  $\mu\text{M}$  PRPP and Gua 50  $\mu\text{M}$  at pH 7.4. The insets show the measurements of enzyme activity at pH 8.5.

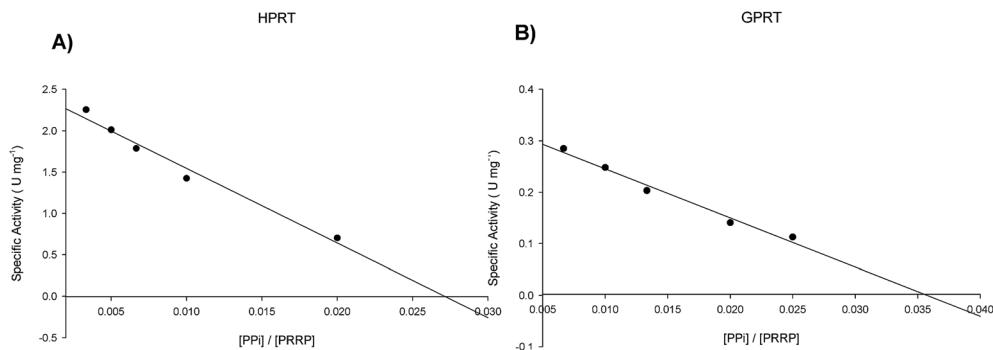


Fig. 7 Plot of enzyme activity against different [PPI]/[PRPP] ratios to determine the equilibrium constant for HPRT (A) and GPRT (B) reactions. The ratios for [IMP]/[Hx] and [GMP]/[Gua] were fixed at 1.

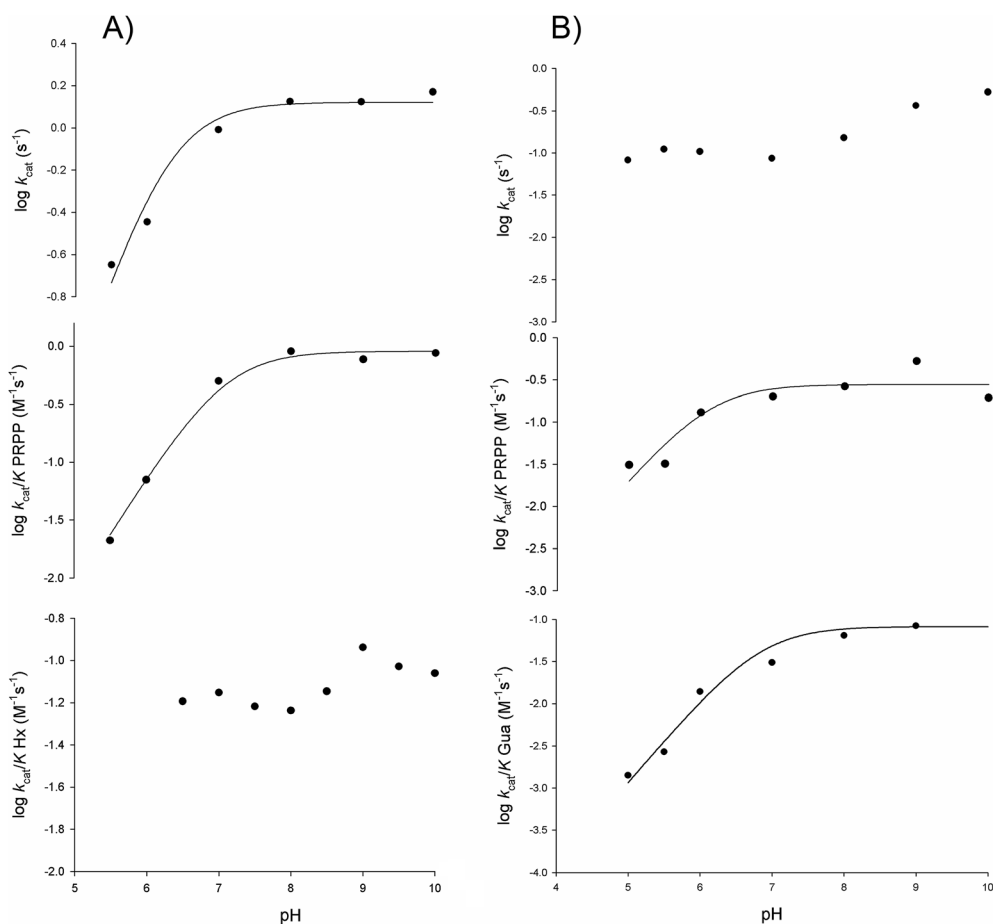


Fig. 8 Dependence of steady-state kinetic parameters on different pH values for HPRT (A) and GPRT (B) reactions.

MtHGPRT is presented in Fig. 9. The transition state shown in Fig. 9 is as proposed by Eads *et al.*<sup>12</sup> based on the HshGPRT crystal structure. These authors propose a transition state with oxocarbenium character at the ribose C1'-O4', with a weak bond to the pyrophosphate group and a weak glycosidic bond between the C1' of ribose and N9 of the purine ring. It is interestingly to point out that Eads *et al.* have proposed that the N7 protonated tautomer of Gua (or Hx) is the species that undergoes catalysis in the forward direction, and that the

Asp137 (Asp126 in MtHGPRT) and Lys165 could play a role in transition-state stabilization *via* protonation or hydrogen bonding at N7.<sup>12</sup> The pH-rate data of  $k_{\text{cat}}$  for HPRT reaction (Fig. 8A) appears to support the proposal that Asp126 plays a role in transition-state stabilization in MtHGPRT.

The pH dependence of  $k_{\text{cat}}/K_{\text{M}}$  relates to the required (or preferred) protonation states for binding and/or subsequent catalysis of groups in either the substrate or the enzyme form it combines with.<sup>44</sup> The data for  $k_{\text{cat}}/K_{\text{PRPP}}$  suggest that an

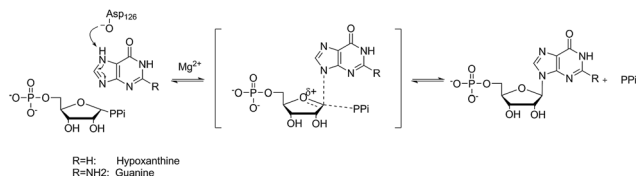


Fig. 9 Proposed chemical mechanism for MthGPRt.

ionizable group with acid dissociation constant of 7.0 for HPRT reaction and 6.1 for GPRT reaction needs to be deprotonated for PRPP binding and/or catalysis (Fig. 8A and B). A highly conserved PRPP binding loop is found in MthGPRt, starting at Val118 and extends to Leu131,<sup>19</sup> and the presence of two acidic amino acid is believed to be critical for PRPP binding to type I PRTases.<sup>25</sup> Interestingly, Xu and Grubmeyer found a bell-shaped profile for  $k_{\text{cat}}/K_{\text{PRPP}}$  data of HshGPRt, suggesting Asp137 as the residue with  $\text{pK}_{\text{a}}$  of 7.1 that needs to be deprotonated and Lys165 as the residue with  $\text{pK}_{\text{a}}$  of 8.8 that needs to be protonated for productive PRPP binding.<sup>43</sup> The authors concluded that Lys165 in human HGPRT (Lys154 in MthGPRt) is involved in ground-state interactions with substrates for nucleotide formation reaction.<sup>43</sup> The crystal structure of MthGPRt in complex with GMP and PPI and  $\text{Mg}^{2+}$  shows that the side chain of Lys154 forms a hydrogen bond with the 6-oxo group of the purine ring, and the authors proposed that this residue plays a role in substrate specificity.<sup>19</sup> However, contrary to the results for human HGPRT,<sup>43</sup> no ionizable group that needs to be protonated was observed in the MthPRT pH-rate profile of  $k_{\text{cat}}/K_{\text{PRPP}}$  (Fig. 8). As the slopes of  $k_{\text{cat}}/K_{\text{PRPP}}$  for HPRT and GPRT reactions were +1, it thus tempting to suggest that the carboxyl side chain of Glu122 or Asp123, which are located in the PRPP binding loop,<sup>19</sup> is the likely residue that needs to be deprotonated for productive PRPP binding for MthGPRt catalysis to occur.

The data for  $k_{\text{cat}}/K_{\text{Gua}}$  of GPRT reaction were fitted to eqn (14), yielding a  $\text{pK}_{\text{a}}$  value of 6.8 ( $\pm 2.0$ ). These results suggest that there is a residue that needs to be deprotonated for productive binding of Gua (Fig. 8B). The side chain of conserved Asp126 has been shown to be rotated away from the N7 of the purine ring of GMP and to form a hydrogen bond with the main chain of nitrogen of Gly128 in the 5'-phosphate binding site.<sup>19</sup> For the HPRT reaction, no equation could be fitted to the  $k_{\text{cat}}/K_{\text{Hx}}$  data (Fig. 8A) and it appears that there is no ionizable group involved in Hx binding in the 5.5 to 10 pH range.

## Conclusions

In this work we present experimental efforts to determine the mode of action of MthGPRt, showing that this enzyme is a type I PRTase. The sequential ordered bi-bi mechanism and the homodimeric quaternary conformation are characteristics of this family of enzymes.<sup>25</sup> MthGPRt is less efficient using either Hx or Gua, when compared to HshGPRt. ITC experiments demonstrated that PRPP, GMP and IMP binds to the free MthGPRt and no binding of Hx or PPI could be observed,

leading to the proposed kinetic mechanism (Fig. 3). Determination of the thermodynamic parameters of MthGPRt-catalyzed chemical reactions suggests a similar overall free activation energy for HPRT and GPRT reactions, and that these reactions proceed at slower rate than predicted by the collision theory. The stopped-flow results suggest that product release participates in the rate-limiting step. SKIE data suggest proton transfer from solvent is not likely involved in the rate-limiting step. Determination of equilibrium constant values for HPRT and GPRT reactions suggest that these processes are not favorable at equilibrium. The analyses of pH-rate profiles indicated that Glu122 and Asp123 residues are likely to play roles in catalysis and/or PRPP binding. These data appear to be borne out by the crystallographic structure of MthGPRt and sequence alignment,<sup>19</sup> showing a conserved PRPP binding motif.<sup>12</sup> Site-directed mutagenesis efforts should thus be pursued to provide a solid basis for the role, if any, of Glu122 and Asp123 in binding and/or catalysis in the mode of action of MthGPRt. In addition, *M. tuberculosis hpt (Rv3624c)* gene replacement efforts should be carried out to evaluate whether or not MthGPRt is essential for growth and/or plays any role in latency. The elucidation of the crystal structure of MthGPRt in complex with products GMP and PPI and  $\text{Mg}^{2+}$  by Eng *et al.*<sup>19</sup> should aid in the design of structure-based enzyme inhibitors. The rational design of enzyme inhibitors should, preferentially, be based on structure and functional data. Accordingly, the results presented here can be useful to these efforts as it provides data on the mode of action of MthGPRt. MthGPRt inhibitors may be both tested as anti-TB agents and used as tools for chemical biologists to carry out loss-of-function experiments to reveal the biological role of MthGPRt in the context of whole *M. tuberculosis* cells.<sup>45</sup>

## Conflict of interest

The authors declare no competing financial interest.

## Acknowledgements

This work was supported by funds awarded by Decit/SCTIE/MSMCT-CNPq-FNDCT-CAPES to National Institute of Science and Technology on Tuberculosis (INCT-TB) to D. S. S. and L. A. B. L. A. B. and D. S. S. also acknowledge financial support awarded by FAPERGS-CNPq-PRONEX-2009. L. A. B. (CNPq, 520182/99-5) and D. S. S. (CNPq, 304051/1975-06) are Research Career Awardee of the National Research Council of Brazil (CNPq). P. C. P., B. L. A., and M. R. acknowledge scholarships awarded by CAPES and CNPq. L. K. B. M. is a Post-Doctoral Fellow of FAPERGS/CAPES.

## References

- 1 World Health Organization, *Global Tuberculosis Report 2013*, WHO Press, Geneva, 2014.
- 2 R. G. Ducati, A. Ruffino-Netto, L. A. Basso and D. S. Santos, *Mem. Inst. Oswaldo Cruz*, 2006, **101**(7), 697–714.



- 3 A. Jain and R. Mondal, *FEMS Immunol. Med. Microbiol.*, 2008, **53**, 145–150.
- 4 A. A. Velayati, P. Farnia, M. R. Masjedi, T. A. Ibrahim and P. Tabarsi, *et al.*, *Eur. Respir. J.*, 2009, **34**, 1202–1203.
- 5 T. R. Rustad, A. M. Sherrid, K. J. Minch and D. R. Sherman, *Cell. Microbiol.*, 2009, **11**, 1151–1159.
- 6 W. Eisenreich, T. Dandekar, J. Heesemann and W. Goebel, *Nat. Rev. Microbiol.*, 2010, **8**, 401–412.
- 7 M. Niederweis, *Microbiology*, 2008, **154**, 679–692.
- 8 K. A. Kantardjieff, C. Vasquez, P. Castro, N. M. Warfel, B. S. Rho, T. Lakin, C. Y. Kim, B. W. Segelke, T. C. Terwilliger and B. Rupp, *Acta Crystallogr., Sect. D: Biol. Crystallogr.*, 2004, **61**, 355–364.
- 9 W. B. Parker and M. C. Long, *Curr. Pharm. Des.*, 2007, **13**, 599–608.
- 10 N. Munagala, V. J. Basus and C. C. Wang, *Biochemistry*, 2001, **40**, 4303–4311.
- 11 D. L. Musick, *Crit. Rev. Biochem.*, 1981, **11**, 1–34.
- 12 J. C. Eads, G. Scapin, Y. Xu, C. Grubmeyer and J. C. Sacchettini, *Cell*, 1994, **78**, 325–334.
- 13 N. R. Munagala, M. S. Chin and C. C. Wang, *Biochemistry*, 1998, **37**, 4045–4051.
- 14 J. P. Page, N. R. Munagala and C. C. Wang, *Eur. J. Biochem.*, 2001, **259**, 565–571.
- 15 Y. Xu, J. Eads, J. C. Sacchettini and C. Grubmeyer, *Biochemistry*, 1997, **36**, 3700–3712.
- 16 L. Yuan, S. P. Craig III, J. H. McKerrow and C. C. Wang, *Biochemistry*, 1992, **31**, 806–810.
- 17 M. A. Wenck, F. J. Medrano, A. E. Eakin and S. P. Craig III, *Biochim. Biophys. Acta*, 2004, **1700**, 11–18.
- 18 G. Biazus, C. Z. Schneider, M. S. Palma, L. A. Basso and D. S. Santos, *Protein Expression Purif.*, 2009, **66**, 185–190.
- 19 W. S. Eng, D. Hocková, P. Spacek, Z. Janeba, N. P. West and K. Woods, *et al.*, *J. Med. Chem.*, 2015, **58**, 4822–4838.
- 20 M. B. Patel, S. P. Kumar, N. N. Valand, Y. T. Jasrai and S. K. Menon, *J. Mol. Model.*, 2013, **19**, 3201–3217.
- 21 I. H. Segel, in *Enzyme kinetics, behavior and analysis of rapid equilibrium and steady-state enzyme systems*, John Wiley and Sons, Inc., New York, 1975, ch. 2, pp. 18–89.
- 22 K. Hiromi, *Kinetics of Fast Enzyme Reactions: Theory and Practice*, Kodansha Ltd., Tokyo, 1979, ch. 4, pp. 188–253.
- 23 T. Lonhienne, E. Baise, G. Feller, V. Bouriotis and C. Gerday, *Biochim. Biophys. Acta*, 2001, **1545**, 349–356.
- 24 P. F. Cook and W. W. Cleland, *Enzyme Kinetics and Mechanism*, Garland Science Publishing, New York, 2007, ch. 9, pp. 253–323.
- 25 S. C. Sinha and J. L. Smith, *Curr. Opin. Struct. Biol.*, 2001, **11**, 733–739.
- 26 J. Victor, A. Leo-Mensah and D. L. Sloan, *Biochemistry*, 1979, **18**, 3597–3604.
- 27 A. Breda, L. A. Rosado, D. M. Lorenzini, L. A. Basso and D. S. Santos, *Mol. Biosyst.*, 2012, **8**, 572–586.
- 28 C. Salerno and A. Giacomello, *J. Biol. Chem.*, 1981, **256**, 3671–3673.
- 29 I. N. S. Subbayya and H. Balaran, *FEBS Lett.*, 2002, **521**, 72–76.
- 30 S. R. Krungkrai, S. Aoki, N. M. Q. Palacpac, D. Sato, T. Mitamura, J. Krungkrai and T. Horii, *Mol. Biochem. Parasitol.*, 2004, **134**, 245–255.
- 31 G. P. Wang, C. Lundegaard, K. F. Jensen and C. Grubmeyer, *Biochemistry*, 1999, **38**, 275–283.
- 32 A. D. Villela, R. G. Ducati, L. A. Rosado, C. J. Bloch, M. V. Prates, D. C. Gonçalves, C. H. I. Ramos, L. A. Basso and D. S. Santos, *PLoS One*, 2013, **8**, e56445.
- 33 P. Kwong, M. L. Doyle, D. J. Casper, C. Cicala, S. A. Leavitt and S. Majeed, *Nature*, 2002, **420**, 678–682.
- 34 J. E. Ladbury and M. L. Doyle, *Bioalorimetry II*, Wiley, London, 2004.
- 35 D. J. Chodera and L. D. Mobley, *Annu. Rev. Biophys.*, 2013, **42**, 121–142.
- 36 D. B. Northrop, *Biochemistry*, 1975, **14**, 2644–2651.
- 37 P. F. Cook, *Enzyme Mechanism from Isotope Effects*, CRC Press, Boca Raton, 1991, pp. 203–228.
- 38 M. P. Patel, W. S. Liu, J. West, D. Tew, T. D. Meek and S. H. Thrall, *Biochemistry*, 2005, **44**(50), 16753–16765.
- 39 R. G. Silva, L. P. S. Carvalho, J. S. Blanchard, D. S. Santos and L. A. Basso, *Biochemistry*, 2005, **45**(43), 13064–13073.
- 40 L. Mascia, M. Cappiello, S. Cherri and P. L. Ipata, *Biochim. Biophys. Acta*, 2000, **1474**, 70–74.
- 41 H. M. Kalckar, *J. Biol. Chem.*, 1947, **167**, 429–443.
- 42 D. J. Porter, *J. Biol. Chem.*, 1992, **267**, 7342–7351.
- 43 Y. Xu and C. Grubmeyer, *Biochemistry*, 1998, **37**, 4114–4124.
- 44 P. F. Cook and W. W. Cleland, *Enzyme Kinetics and Mechanism*, Garland Science Publishing, New York, 2007, ch. 10, pp. 325–366.
- 45 A. C. Bishop and V. L. Chen, *J. Chem. Biol.*, 2009, **2**, 1–9.